

ARTICLE

Open Access

# Ultrabroadband absorptive refractory plasmonics for photocatalytic hydrogen evolution reactions

Myeongcheol Go<sup>1,2</sup>, Inju Hong<sup>1,3</sup>, Dasol Lee<sup>4</sup>, Sanghoon Kim<sup>1,2</sup>, Junho Jang<sup>1,2</sup>, Keon-Woo Kim<sup>1,2</sup>, Sangmin Shim<sup>4</sup>, Kijung Yong<sup>1,3</sup>, Junsuk Rho<sup>1,5,6</sup> and Jin Kon Kim<sup>1,2</sup>

## Abstract

As an environmentally friendly and renewable method for hydrogen production powered by solar energy, photocatalytic hydrogen evolution reactions (HERs) using broadband absorbers have received much attention. Here, we report the fabrication and characterization of an ultrabroadband absorber for the photocatalytic HER. The absorber is composed of titanium nitride and titanium dioxide heterostructures deposited onto a porous anodized aluminum oxide template. The absorber shows ultrabroadband absorption in both the visible and near-infrared regions (400–2500 nm), with averages of 99.1% and 80.1%, respectively. Additionally, the presence of the TiO<sub>2</sub> layer within the absorber extends the lifetime of the hot carriers by 2.7 times longer than that without the TiO<sub>2</sub> layer, enhancing the transfer of hot electrons and improving the efficiency of hydrogen production by 1.9 times. This novel ultrabroadband absorber has potential use in advanced photocatalytic HER applications, providing a sustainable and cost-effective route for hydrogen generation from solar energy.

## Introduction

The photocatalytic hydrogen evolution reaction (HER) has received much attention due to hydrogen generation in an environmentally friendly and renewable way using solar energy without external input<sup>1–5</sup>. The absorption of light leads to the generation of “hot carriers” composed of hot electrons and hot holes<sup>6</sup>. These hot electrons can then reduce H<sup>+</sup> into hydrogen gas, providing a conversion of solar energy into hydrogen energy. Platinum-based materials have been widely used because of their high activity and stability<sup>7–9</sup>. However, their high cost remains challenging, and alternative materials that are abundant, cheaper, and can effectively catalyze HER are needed.

Potential alternatives include transition metals such as metal nitrides, sulfides, and carbides<sup>10–12</sup>. Additionally, an efficient photocatalytic system requires broadband absorption of the solar spectrum to generate more hot carriers<sup>13,14</sup>, with a prolonged lifetime and their fabrication over a large area.

Plasmonic refractory metals, such as titanium nitride (TiN), zirconium nitride, and hafnium nitride, provide enhanced thermal stability and mechanical strength at high temperatures compared with noble metals (gold and silver)<sup>15–19</sup>. Among them, TiN has received much attention because its optical properties are comparable to those of noble metals in visible and near-infrared (NIR) regions. However, TiN does not have effective absorption of NIR wavelengths, which accounts for 50% of the solar spectrum<sup>20</sup>. When TiN is combined with anodized aluminum oxide (AAO), it shows ultrabroadband absorption covering the entire solar spectrum<sup>21–23</sup>. Furthermore, TiN has fast hot electron-hot hole recombination, which makes it suitable for photothermal devices<sup>24</sup>. Therefore, these characteristics are suitable for use in solar-driven water purification utilizing the photothermal effect<sup>21,22</sup>. On the

Correspondence: Kijung Yong (kyong@postech.ac.kr) or Junsuk Rho (jsrho@postech.ac.kr) or Jin Kon Kim (jkkim@postech.ac.kr)

<sup>1</sup>Department of Chemical Engineering, Pohang University of Science and Technology (POSTECH), Pohang 37673, Republic of Korea

<sup>2</sup>National Creative Research Initiative Center for Hybrid Nano Materials by High-level Architectural Design of Block Copolymer, Department of Chemical Engineering, Pohang University of Science and Technology, Pohang 37673, Republic of Korea

Full list of author information is available at the end of the article

These authors contributed equally: Myeongcheol Go, Inju Hong, Dasol Lee

© The Author(s) 2024



**Open Access** This article is licensed under a Creative Commons Attribution 4.0 International License, which permits use, sharing, adaptation, distribution and reproduction in any medium or format, as long as you give appropriate credit to the original author(s) and the source, provide a link to the Creative Commons license, and indicate if changes were made. The images or other third party material in this article are included in the article's Creative Commons license, unless indicated otherwise in a credit line to the material. If material is not included in the article's Creative Commons license and your intended use is not permitted by statutory regulation or exceeds the permitted use, you will need to obtain permission directly from the copyright holder. To view a copy of this license, visit <http://creativecommons.org/licenses/by/4.0/>.

other hand, for applications in photocatalysts including HER, prolonging the recombination time of the hot carriers is crucial because the increased lifetime of hot carriers enhances the mean free path of the hot electrons, resulting in improved participation in HER<sup>11,25–27</sup>. Creating heterostructures by combining two different materials (for instance, metal and semiconductor) can aid in the effective separation of the electron-hole pairs because hot electrons generated at the metal can be transferred to the semiconductor's conduction band. For this reason, TiN/TiO<sub>2</sub> nanoparticles have been widely used as photocatalysts<sup>28–30</sup>. However, because these nanoparticles do not show ultrabroadband absorption, obtaining ultrabroadband absorption for effective photocatalysts remains a challenge.

In this study, we fabricated an ultrabroadband absorber by consecutively depositing TiO<sub>2</sub> and TiN onto a porous AAO template and utilized it in the photocatalytic HER. By optimizing the TiN deposition, we enhanced absorption in the visible and NIR regions. The fabricated absorber has a very high average absorption of 99.1% in the visible (400–700 nm) region and 80.1% in the NIR (700–2500 nm) region. Using the finite-difference time-domain (FDTD) method, the enhanced absorption effectively matched the experimental results. In addition, the absorber structure incorporating the TiN/TiO<sub>2</sub> junction could extend the lifetime of hot carriers by 2.7 times; this affected the hydrogen production rate, which was enhanced by more than 1.9 times compared to that without the TiO<sub>2</sub> layer.

## Materials and methods

### Sample fabrication

A free-standing AAO membrane was prepared using two-step anodization. A highly pure aluminum sheet (99.999%, 1 mm thick) was sonicated in acetone for 30 min and then electrochemically polished in a mixed solution of perchloric acid and ethanol (1:4 v/v) at 7 °C and 20 V for 30 min. The polished aluminum plate was alternately washed with ethanol and deionized (DI) water. The first anodization was carried out with 0.1 M phosphoric acid (H<sub>3</sub>PO<sub>4</sub>) aqueous solution at 0 °C and 195 V for 16 h, etched by an etchant solution (1.8 wt% chromic acid (H<sub>2</sub>CrO<sub>4</sub>) and 6 wt% H<sub>3</sub>PO<sub>4</sub> in deionized water) at 65 °C for over 6 h and washed with DI water. The second anodization was performed under the same conditions as the first anodization solution. The interpore distance between two neighboring pores in the AAO template was 500 nm. Finally, the pores were enlarged in 0.1 M phosphoric acid to diameters of 470 nm, and then the sample was rinsed with DI water. TiO<sub>2</sub> was deposited using atomic layer deposition (ALD, Plus 200, QUROS) at 230 °C. TiN was deposited using sputtering (E5500, AMAT) at 200 °C.

### Characterization

A UV-VIS-NIR spectrometer (Lambda 750 S, PerkinElmer) with 60 mm integrating sphere modules was used to characterize the absorption of samples in the wavelength range of 400–2500 nm. For reference, the white reflectance standard (Ocean optics) was used. We defined absorption as 1-reflectance. The fabricated samples were observed by a scanning electron microscope (SEM, Hitachi S4800). The lifetime of the hot electron of the absorbers was measured by a spectrophotofluorometer (MicroTime-200, Picoquant). Spectroscopic ellipsometry (V-VASE, J.A. Woollam) was used to extract the optical properties of the TiN layer in the wavelength range of 300–2500 nm.

### Photocatalytic H<sub>2</sub> production measurements

The samples were prepared in 1 × 1 cm<sup>2</sup> size for hydrogen production. Photocatalytic H<sub>2</sub> production experiments were performed by immersing the sample in water containing 10% triethanolamine (TEOA), which was the sacrificial reagent, in a 30 ml sealed Pyrex reactor using a magnetic stirrer set at a constant rotational speed. Before light irradiation, argon gas was purged through the reactor for 30 min to eliminate any residual air. A 300 W Xe lamp (Oriel) was used as the light source; the incident power of the Xe lamp was measured using a power meter (12 A, Ophir). The produced gas was collected and analyzed by gas chromatography (GC, Agilent 7890A-5975C, with nitrogen as the carrier gas) equipped with a thermal conductivity detector.

## Results and discussion

We fabricated an ultrabroadband absorber by sequentially depositing TiO<sub>2</sub> and TiN on a porous AAO template, as schematically illustrated in Fig. 1a. First, an AAO template with a height of 10 μm, a distance between two neighboring pores of 500 nm, and a pore diameter of 470 nm was fabricated using the two-step anodization method and widening process<sup>31–33</sup>. Then, TiO<sub>2</sub> (5 nm) was deposited on the AAO template through ALD. Finally, TiN was deposited with sputtering. The top and tilted SEM images of the fabricated absorber are shown in Fig. 1b, c, respectively. These processes were also observed using energy-dispersive X-ray spectroscopy (Fig. S1). After depositing the TiO<sub>2</sub> layer, we observed an increase in the amount of titanium (Ti). Similarly, after sputtering the TiN layer, the nitrogen (N) component was increased. Finally, we fabricated an ultrabroadband absorber over a large area (5 × 5 cm<sup>2</sup>) (Fig. 1d).

Ultrabroadband absorbers with different TiN thicknesses (0–60 nm) were prepared (Fig. 2a–d). With increasing thickness of the TiN layer, the pore size gradually decreased. We obtained the depth profile of titanium, nitrogen, aluminum (Al), and oxygen (O) elements

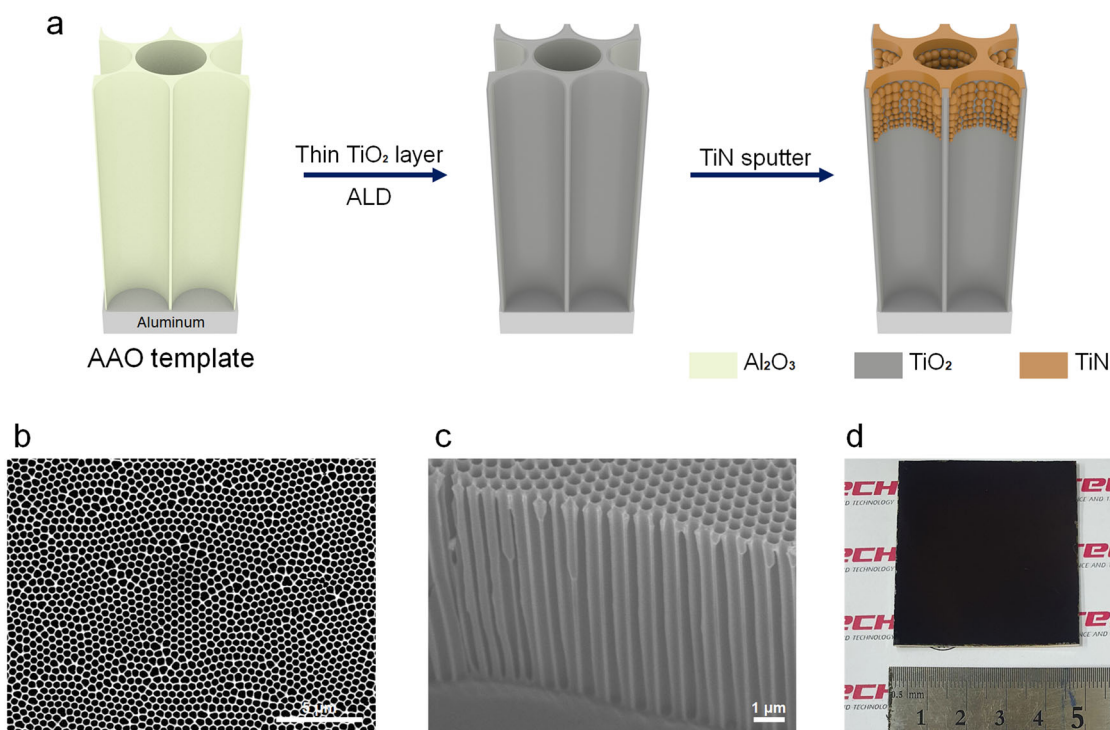


**Fig. 1 Fabrication of the ultrabroadband absorber.** **a** Schematic of the fabrication step of the ultrabroadband absorber. **b** Top and **c** tilted SEM images of the absorber. **d** Photograph of the fabricated absorber over a large area ( $5 \times 5 \text{ cm}^2$ ).

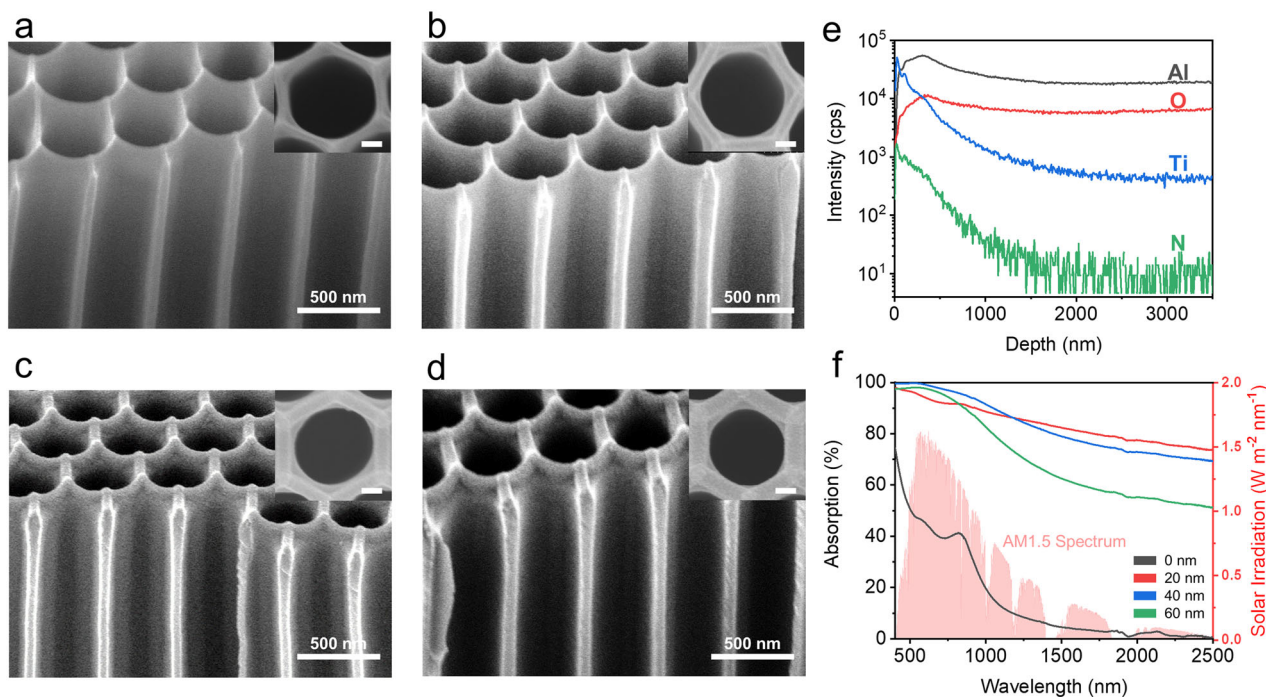


**Fig. 2 Characterization of the ultrabroadband absorber.** SEM images of ultrabroadband absorbers with different deposition thicknesses of TiN: **a** 0 nm, **b** 20 nm, **c** 40 nm, and **d** 60 nm. (scale bar in inset image = 100 nm). **e** Depth profile of the atomic elements (Al, O, Ti, N) in the absorber. **f** Absorption spectrum of the absorbers with different TiN thicknesses and AM1.5 standard solar irradiation spectrum.

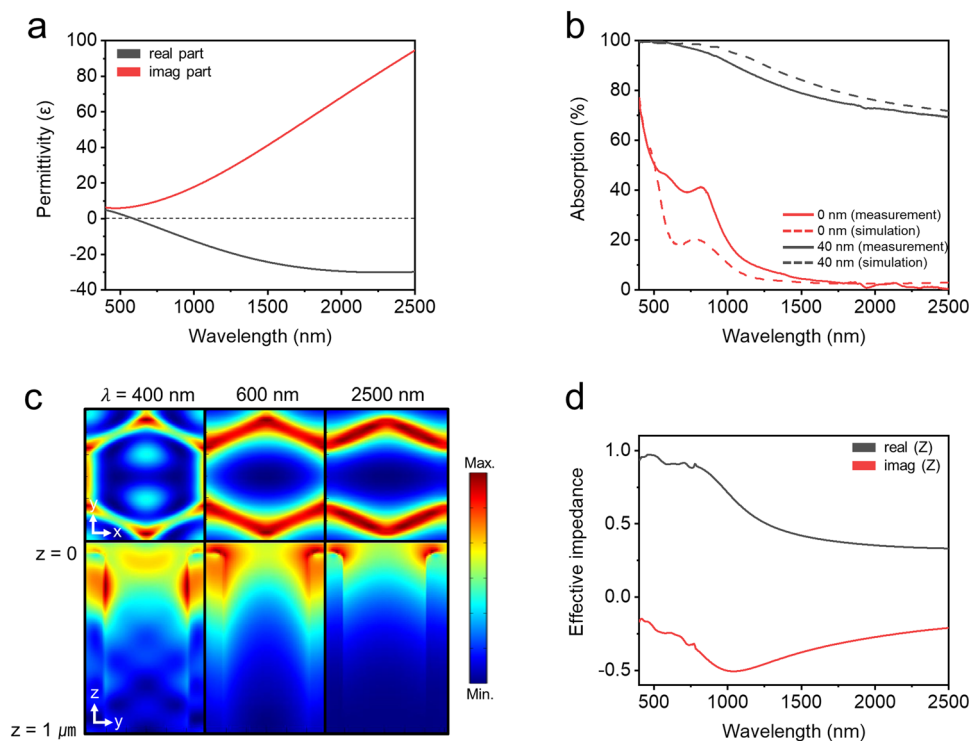


**Fig. 3** Simulation of the ultrabroadband absorber. **a** Permittivity of TiN. **b** Measured and simulated absorptions of the two absorbers. **c** Simulated magnetic field distribution of the xy-plane (top) and yz-plane (bottom) at wavelengths of 400, 600, and 2500 nm. **d** Effective impedance of the absorber with a 40 nm TiN layer retrieved from the S-parameters.

through secondary ion mass spectrometry (SIMS) (Fig. 2e). ALD is capable of deposition at a high aspect ratio; while the composition of  $\text{TiO}_2$  deposited via ALD was maintained at the bottom of AAO, the nitrogen component rapidly decreased with increasing depth. Hence, TiN was deposited as particles only near the opening of AAO. Figure 2f shows the absorption spectra of the absorbers with different TiN thicknesses. When no TiN layer was on the AAO, the average absorption was 50.0% in the visible (400–700) range and 9.6% in the NIR (700–2500) range. When the TiN thickness was 20 nm, the average absorption dramatically increased to 95.2% in the visible range and 82.0% in the NIR range. Another absorber with a 40 nm TiN layer showed an increased absorption (99.1%) in the visible range, with a slight decrease in absorption (80.1%) in the NIR range. However, with a further increase in the TiN layer (60 nm), the average absorption decreased (97.5% in the visible range and 65.7% in the NIR region). This occurred because when excessive TiN was deposited, a thick TiN layer was also formed on the top surface of the AAO, resulting in a reduction in the nanopore size. Additionally, the existence of thicker TiN layers on the top surface of AAO increased the reflectance. Thus, when the thickness of the TiN layer was above 40 nm, the average absorption was significantly

reduced. Thus, the absorber with a 40 nm TiN layer showed the best absorption considering the solar spectrum over the entire wavelength.

The enhanced absorption of an absorber with a 40 nm TiN layer was also confirmed through FDTD simulation, as shown in Fig. 3. The refractive index of TiN in the range of 400–2500 nm was obtained through ellipsometry (Fig. S2). The permittivity was then fitted using the Drude-Lorentz model, as follows:

$$\epsilon(\omega) = \epsilon_{\infty} - \frac{\omega_p^2}{\omega^2 - i\omega\Gamma_D} - \sum_{j=1}^N \frac{f_j \omega_p^2}{\omega_{0j}^2 - \omega^2 - i\omega\Gamma_j}$$

where  $\epsilon_{\infty}$  is the background permittivity,  $\omega_p$  is the plasmon frequency,  $\Gamma_D$  and  $\Gamma_j$  are the Drude and Lorentz damping rates, respectively, and  $f_j$  is the strength of the Lorentz oscillator (Fig. 3a). FDTD modeling was based on the SIMS data and SEM images; here, TiN was deposited within the openings of AAO, while  $\text{TiO}_2$  was deposited throughout the entire AAO template. The simulated absorption was similar to the experiment (Fig. 3b). To understand the enhanced absorption over a wide range of wavelengths, we calculated the magnetic field distributions at wavelengths of 400, 600, and 2500 nm. High absorption is associated with the plasmon dark mode



within the absorber<sup>34</sup>. The excitation of the dark mode has been reported to generate hot electrons in various absorbers<sup>35,36</sup>. The plasmon dark mode arises from the out-of-phase oscillation of the conduction electrons within the metallic nanostructure<sup>37,38</sup>. The excitation of a nonradiative dark plasmon occurs due to the compensation of the dipole moment of the unit cell. The dark mode can exhibit broadband characteristics due to its weak nonresonant frequency dependence. The dark mode represents a pattern of mirror symmetry in the field distribution, as shown in Fig. 3c, where the calculated magnetic field distribution exhibits mirror symmetry over a wide range of wavelengths. At 400 nm, strong magnetic resonance occurred in the hexagonal apexes on the xy-plane and reached ~200 nm deep in the yz-plane. At 600 nm, resonance occurred in the openings and slightly shallower wall surfaces. However, at 2500 nm, a strong magnetic resonance was observed only in the open regions. These results indicated that both the magnetic field and absorbed power density were highly concentrated in the gap between the AAO pores. The presence of the TiN layer near the surface-enhanced the excitation of magnetic dipole resonance due to the reduced scattering in the subwavelength region. As a result, absorption occurred over a broad range of wavelengths, facilitated by the distribution of the magnetic field at the specific wavelength<sup>39</sup>. This broadband absorption arising from various locations would induce the creation of more hot electrons from diverse regions.

We determined the effective impedance of the suggested structure (Fig. 3d) by impedance matching of the absorbers with the S-parameter retrieval methods<sup>40,41</sup>:

$$z = \pm \sqrt{\frac{(1 + S_{11})^2 - S_{21}^2}{(1 - S_{11})^2 - S_{21}^2}}$$

where  $S_{11}$  and  $S_{21}$  are the reflection and transmission properties of electromagnetic devices, respectively. The effective impedance of the absorber shows that the real part is close to 1 and the imaginary part is close to 0. Thus, the impedance of the proposed structure is approximately equal to the impedance of free space, indicating an efficient acquisition of the electromagnetic waves from the surrounding air. This impedance match ensures optimal absorption with minimal reflected waves. The real part with a value near 1 signifies that the majority of the wave's energy is absorbed, while the imaginary part with a value near zero corresponds to minimal reactive energy, indicating that the wave is not significantly stored or delayed within the material; this is a trait of an ideal absorber.

To investigate the role of  $\text{TiO}_2$  in the absorber, we prepared TiN +  $\text{TiO}_2$  on the AAO absorber, TiN on the AAO absorber, and a TiN film without AAO. TiN on the

AAO absorber was fabricated by depositing TiN alone on AAO. The absorption of TiN +  $\text{TiO}_2$  on the AAO absorber and TiN on the AAO absorber was almost identical (Fig. 4a). These results indicated that the existence of a thin  $\text{TiO}_2$  layer (5 nm) did not affect light absorption. However, the average lifetime of the hot electrons showed a large difference (4.81 ns for TiN +  $\text{TiO}_2$  on the AAO absorber, 1.80 ns for TiN on the AAO absorber, and 0.643 ns for the TiN film) (Fig. 4b). Thus, the addition of a thin  $\text{TiO}_2$  layer showed 2.7 times and 7.5 times prolonged hot electron lifetimes compared to TiN on the AAO absorber and TiN film, respectively. This occurred because some of the hot electrons excited above the conduction band of TiN were easily transferred to the  $\text{TiO}_2$  layer<sup>10,42,43</sup>. These hot electrons could not crossover to the  $\text{Al}_2\text{O}_3$  layer due to the insulator, and they recombined with hot holes in the  $\text{TiO}_2$  and TiN layers. (Fig. 4c. i). For TiN on the AAO absorber, most of the hot electrons generated in the TiN layer could not transfer to the  $\text{Al}_2\text{O}_3$  layer and were immediately recombined (Fig. 4c. ii). For the TiN flat film, which did not have a good transferable layer, such as  $\text{Al}_2\text{O}_3$  (Fig. 4c. iii), the lifetime of the hot electrons was shorter (Fig. 4c. iii).

We conducted the hydrogen evolution reaction using different absorbers. First, each absorber was cut into  $1 \times 1 \text{ cm}^2$  pieces, placed in an aqueous TEOA solution, and irradiated by a xenon (Xe) lamp. For TiN+ $\text{TiO}_2$  on the AAO absorber, the hot electrons generated by the absorption of light in the TiN layer were easily transferred into the  $\text{TiO}_2$  layer, reducing  $\text{H}^+$  to produce  $\text{H}_2$  (the schematic is shown in Fig. 5a). The remaining holes in the TiN layer were consumed by oxidizing TEOA (a hole scavenger) to  $\text{TEOA}^+$  (Fig. 5a). The volume fraction of TEOA in water was 10 vol % because the  $\text{H}_2$  evolution reaction rate reached a maximum at this concentration (Fig. S3).

With increasing irradiation time of light, hydrogen production steadily increased (Fig. 5b). No hydrogen was produced without light because the hot electrons were only generated by the light absorption in the TiN layer. Figure 5c shows the hydrogen production of different absorbers with irradiation lasting up to 5 h. The average  $\text{H}_2$  evolution rate of TiN +  $\text{TiO}_2$  on the AAO absorber was the highest ( $12.5 \mu\text{mol}/\text{cm}^2\text{h}$ ), followed by  $\text{TiO}_2$  on AAO ( $6.9 \mu\text{mol}/\text{cm}^2\text{h}$ ), TiN on AAO ( $6.6 \mu\text{mol}/\text{cm}^2\text{h}$ ), and TiN film ( $1.8 \mu\text{mol}/\text{cm}^2\text{h}$ ). AAO itself did not produce any hydrogen because the insulator AAO could not generate hot electrons when exposed to sunlight. In the case of the TiN film, hydrogen reactions could occur on the surface of the TiN layer. TiN alone could facilitate the  $\text{H}_2$  evolution reaction through the interband transitions from N p to Ti  $d_{t2g}$  orbitals<sup>28,44</sup>. TiN on the AAO absorber produced more hydrogen than the TiN film due to increased hot electron generation caused by the

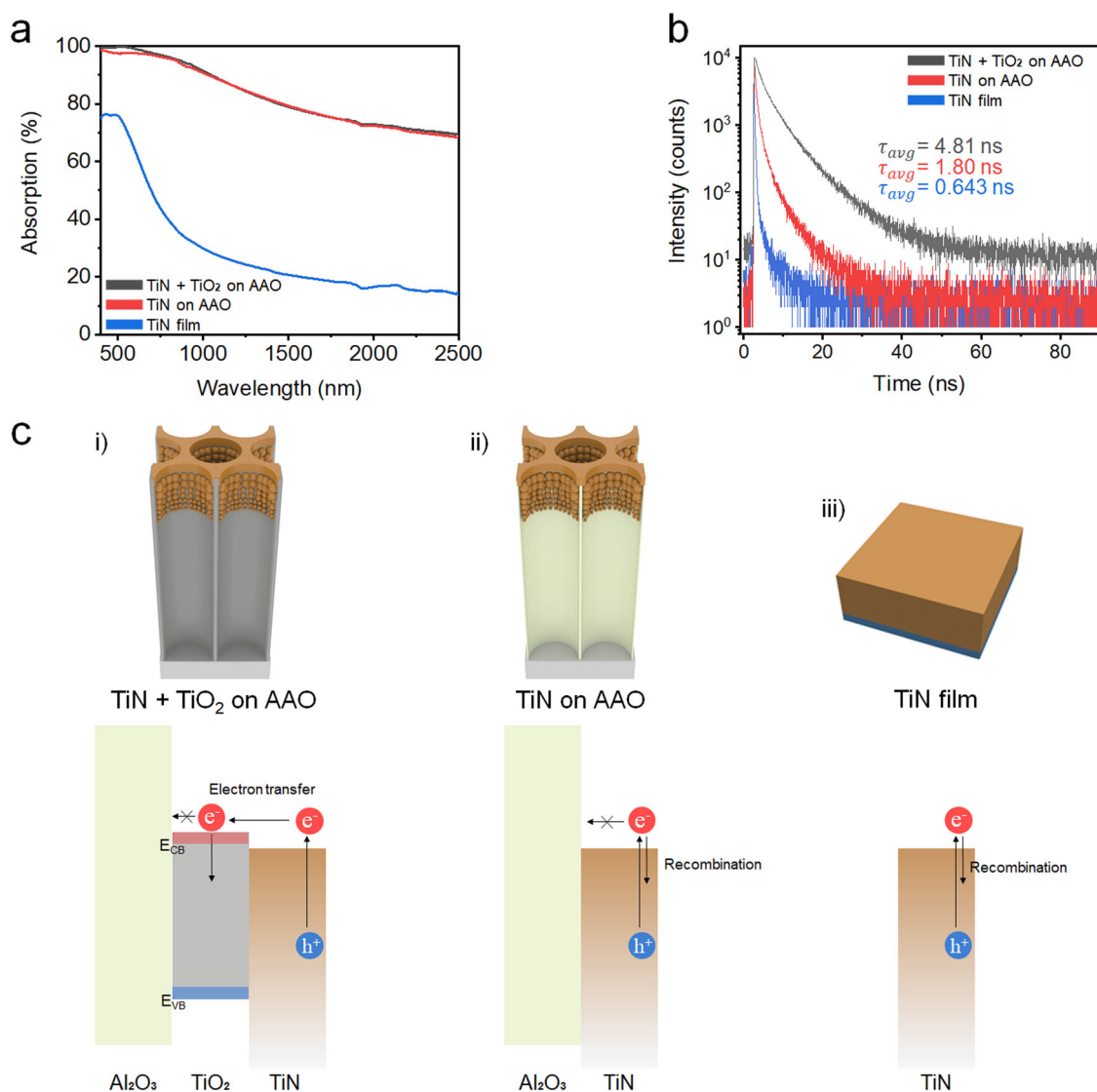


**Fig. 4** Hot electron transfer of the absorbers. **a** Absorption spectra and **b** time-resolved photoluminescence of three absorbers: TiN + TiO<sub>2</sub> on AAO, TiN on AAO, and TiN film. **c** Schematic of the structures and electron transfer of the three absorbers.

enhanced broadband absorption of TiN on AAO. Interestingly, although TiO<sub>2</sub> on AAO showed lower absorption than TiN on the AAO absorber, it also showed slightly higher hydrogen production. This occurred because TiN had a higher adsorption-free energy for hydrogen, leading to increased endothermic dissociation of the hydrogen molecules compared to TiO<sub>2</sub><sup>28</sup>. Consequently, the hydrogen production reaction rate of TiN was lower than that of TiO<sub>2</sub>.

The TiN+TiO<sub>2</sub> on the AAO absorber had a 1.8-fold increase in hydrogen production compared to TiO<sub>2</sub> on the AAO absorber and a 1.9-fold increase in hydrogen production compared to TiN on the AAO absorber. The increased hydrogen production of TiN+TiO<sub>2</sub> on the AAO absorber was caused by the combined effects of the catalytic role of

the TiO<sub>2</sub> layer in hydrogen generation, the enhancement of the hot electron lifetime, and the increased ultrabroadband absorption of the TiN layer. Finally, a cycling test (5 cycles with 1 h for each cycle) of TiN+TiO<sub>2</sub> on the AAO absorber and TiO<sub>2</sub> on the AAO absorber for the H<sub>2</sub> evolution reaction was performed (Fig. 5d). TiN+TiO<sub>2</sub> on the AAO absorber showed higher hydrogen evolution than TiO<sub>2</sub> on AAO. In addition, after 5 cycles, the retention of the hydrogen evolution reaction was still high (~84%) for both samples. Additionally, TiN+TiO<sub>2</sub> on the AAO absorber did not show any damage or detachment from the TiO<sub>2</sub> layer after 5 cycles; this result was attributed to the strong chemical resistance of TiN (Fig. S4). Thus, this absorber was suitable for hydrogen production reactions. The TiN+TiO<sub>2</sub> on the AAO absorber introduced in this study could be used

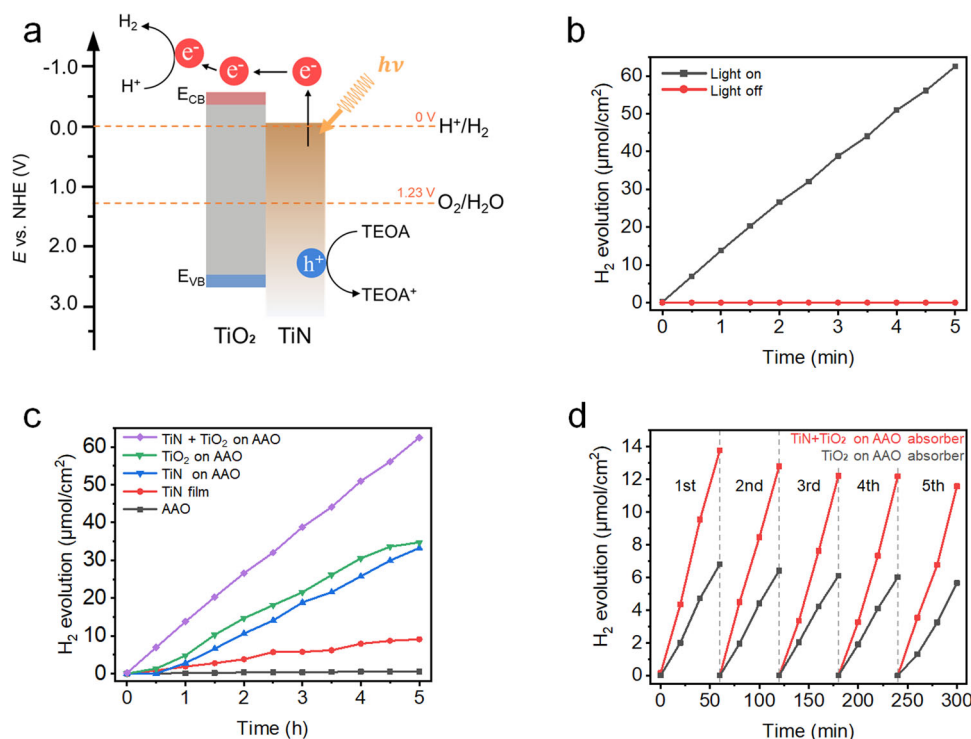


**Fig. 5** H<sub>2</sub> evolution reaction of the ultrabroadband absorber. **a** Schematic of the mechanism of the photocatalytic H<sub>2</sub> evolution reaction of the absorber. **b** H<sub>2</sub> evolution of TiN+TiO<sub>2</sub> on the AAO absorber upon irradiation time with and without light. **c** H<sub>2</sub> evolution of different absorbers: TiN+TiO<sub>2</sub> on AAO, TiO<sub>2</sub> on AAO, TiN on AAO, TiN film, and AAO template. **d** Cycling tests of the H<sub>2</sub> evolution reaction on TiN+TiO<sub>2</sub> on the AAO absorber and TiO<sub>2</sub> on the AAO absorber.

for sustainable and cleaner hydrogen production, utilizing solar energy.

## Conclusions

We fabricated an ultrabroadband absorber for photocatalytic HERs. The absorber with TiN and TiO<sub>2</sub> heterostructures on an AAO template showed ultrabroadband absorption, covering both the visible and near-infrared regions. The incorporation of the TiO<sub>2</sub> layer extended the lifetime of hot carriers by 2.7 times, leading to improved electron transfer and enhanced hydrogen production efficiency by 1.9 times compared to that without the TiO<sub>2</sub> layer. This novel absorber could be used for cost-effective hydrogen production utilizing environmentally friendly and renewable solar energy.

## Acknowledgements

J.K.K. acknowledges financial support from the National Creative Research Initiative Program (NRF-2022R1A3A3002149). J.R. acknowledges the POSCO-POSTECH-RIST Convergence Research Center program funded by POSCO and National Research Foundation (NRF) grants (NRF-2022M3C1A3081312, NRF-2022K1A3A1A25081970, NRF-2019R1A2C3003129, NRF-2019R1A5A8080290) funded by the Ministry of Science and ICT (MSIT) of the Korean government. D.L. acknowledges the NRF grant (NRF-2022R1F1A1065453) funded by the MSIT and Regional Innovation Strategy (RIS) through the NRF funded by the Ministry of Education (MOE) in 2023 (2022RIS-005) of the Korean government. K.Y. was financially supported by the National Research Foundation of Korea

(NRF) grant funded by the Korean Government (MSIT) (NRF-2021R1A5A1084921, NRF-2021K1A4A8A02079226).

## Author details

<sup>1</sup>Department of Chemical Engineering, Pohang University of Science and Technology (POSTECH), Pohang 37673, Republic of Korea. <sup>2</sup>National Creative Research Initiative Center for Hybrid Nano Materials by High-level Architectural Design of Block Copolymer, Department of Chemical Engineering, Pohang University of Science and Technology, Pohang 37673, Republic of Korea. <sup>3</sup>Surface Chemistry Laboratory of Electronic Materials, Department of Chemical Engineering, POSTECH, Pohang 37673, Republic of Korea. <sup>4</sup>Department of Biomedical Engineering, Yonsei University, Wonju 26493, Republic of Korea. <sup>5</sup>Department of Mechanical Engineering, Pohang University of Science and Technology (POSTECH), Pohang 37673, Republic of Korea. <sup>6</sup>POSCO-POSTECH-RIST Convergence Research Center for Flat Optics and Metaphotonics, Pohang 37673, Republic of Korea

## Author contributions

M.G. and I.H. conceived the idea. M.G. fabricated the absorber. I.H. performed the HER experiment. D.L. and S.S. conducted the numerical simulation. M.G., I.H., D.L., S.K., J.J., and K.K. prepared the manuscript. K.Y., J.R., and J.K.K. supervised the project. All authors participated in the discussion and approved the final manuscript.

## Conflict of interest

The authors declare no competing interests.

## Publisher's note

Springer Nature remains neutral with regard to jurisdictional claims in published maps and institutional affiliations.

**Supplementary information** The online version contains supplementary material available at <https://doi.org/10.1038/s41427-023-00523-7>.

Received: 14 August 2023 Revised: 15 November 2023 Accepted: 24 November 2023.

Published online: 19 January 2024

## References

- Yang, J.-L. et al. Boosting Photocatalytic Hydrogen Evolution Reaction Using Dual Plasmonic Antennas. *ACS Catalysis* **11**, 5047–5053 (2021).
- Zhu, Q., Xu, Z., Qiu, B., Xing, M. & Zhang, J. Emerging Cocatalysts on G-C<sub>3</sub>N<sub>4</sub> for Photocatalytic Hydrogen Evolution. *Small* **17**, 2101070 (2021).
- Liu, H., Wang, T. & Zeng, H. Cupns for Efficient Photocatalytic Hydrogen Evolution. *Particle & Particle Systems Characterization* **32**, 869–873 (2015).
- Lau, V. W.-H. et al. Urea-Modified Carbon Nitrides: Enhancing Photocatalytic Hydrogen Evolution by Rational Defect Engineering. *Advanced Energy Materials* **7**, 1602251 (2017).
- Hong, I., Chen, Y.-A., Hsu, Y.-J. & Yong, K. Triple-Channel Charge Transfer over W<sub>18</sub>O<sub>49</sub>/Au/G-C<sub>3</sub>N<sub>4</sub> Z-Scheme Photocatalysts for Achieving Broad-Spectrum Solar Hydrogen Production. *ACS Applied Materials & Interfaces* **13**, 52670–52680 (2021).
- Zhang, Y. et al. Surface-Plasmon-Driven Hot Electron Photochemistry. *Chemical Reviews* **118**, 2927–2954 (2018).
- Li, Y. et al. In Situ Photodeposition of Platinum Clusters on a Covalent Organic Framework for Photocatalytic Hydrogen Production. *Nature Communications* **13**, 1355 (2022).
- Wang, D., Liu, Z.-P. & Yang, W.-M. Revealing the Size Effect of Platinum Cocatalyst for Photocatalytic Hydrogen Evolution on TiO<sub>2</sub> Support: A Dft Study. *ACS Catalysis* **8**, 7270–7278 (2018).
- Dang, T. T. et al. Oxidized Platinum Cocatalyst and Self-Assembled Graphene over Graphitic Carbon Nitride for Photocatalytic Hydrogen Evolution. *ACS Applied Nano Materials* **6**, 9825–9838 (2023).
- Naldoni, A. et al. Broadband Hot-Electron Collection for Solar Water Splitting with Plasmonic Titanium Nitride. *Advanced Optical Materials* **5**, 1601031 (2017).
- Jiang, M. et al. Hot-Electron Injection and Charge Carrier Lifetime Prolongation Enhance the Photoelectrochemical Performance of a Plasmonic Cds/Au Photoanode. *The Journal of Physical Chemistry C* **125**, 17109–17116 (2021).
- Liu, J. et al. Metal-Free Efficient Photocatalyst for Stable Visible Water Splitting Via a Two-Electron Pathway. *Science* **347**, 970–974 (2015).
- Xiao, Q. et al. Hot-Carrier Organic Synthesis Via the near-Perfect Absorption of Light. *ACS Catalysis* **8**, 10331–10339 (2018).
- Loh, J. Y. Y. et al. Near-Perfect Absorbing Copper Metamaterial for Solar Fuel Generation. *Nano Letters* **21**, 9124–9130 (2021).
- Lalisse, A., Tessier, G., Plain, J. & Baffou, G. Plasmonic Efficiencies of Nanoparticles Made of Metal Nitrides (Tin, Zrn) Compared with Gold. *Scientific Reports* **6**, 38647 (2016).
- Diroll, B. T., Saha, S., Shalaeve, V. M., Boltasseva, A. & Schaller, R. D. Broadband Ultrafast Dynamics of Refractory Metals: Tin and Zrn. *Advanced Optical Materials* **8**, 2000652 (2020).
- Guo, W.-P. et al. Titanium Nitride Epitaxial Films as a Plasmonic Material Platform: Alternative to Gold. *ACS Photonics* **6**, 1848–1854 (2019).
- Ijaz, S. et al. Exploiting Zirconium Nitride for an Efficient Heat-Resistant Absorber and Emitter Pair for Solar Thermophotovoltaic Systems. *Opt. Express* **29**, 31537–31548 (2021).
- Chang, C.-C. et al. Highly Plasmonic Titanium Nitride by Room-Temperature Sputtering. *Scientific Reports* **9**, 15287 (2019).
- Escobedo, J. F., Gomes, E. N., Oliveira, A. P. & Soares, J. Ratios of Uv, Par and Nir Components to Global Solar Radiation Measured at Botucatu Site in Brazil. *Renewable Energy* **36**, 169–178 (2011).
- Traver, E. et al. Tin, Zrn, and Hfn Nanoparticles on Nanoporous Aluminum Oxide Membranes for Solar-Driven Water Evaporation and Desalination. *ACS Applied Nano Materials* **3**, 2787–2794 (2020).
- Kaur, M., Ishii, S., Shinde, S. L. & Nagao, T. All-Ceramic Solar-Driven Water Purifier Based on Anodized Aluminum Oxide and Plasmonic Titanium Nitride. *Advanced Sustainable Systems* **3**, 1800112 (2019).
- Chang, C.-C., Kuo, S.-C., Cheng, H.-E., Chen, H.-T. & Yang, Z.-P. Broadband Titanium Nitride Disordered Metasurface Absorbers. *Opt. Express* **29**, 42813–42826 (2021).
- Diroll, B. T. et al. Photothermal Behaviour of Titanium Nitride Nanoparticles Evaluated by Transient X-Ray Diffraction. *Nanoscale* **13**, 2658–2664 (2021).
- Li, H. et al. Self-Assembly of Carbon Black/Aao Templates on Nanoporous Si for Broadband Infrared Absorption. *ACS Applied Materials & Interfaces* **12**, 4081–4087 (2020).
- Yang, Y. et al. Prolonging the Lifetimes of Plasmonic Hot Electrons for Efficient Hydrogen Evolution by Ag@N,O-C Interfaces with a Unique Ginkgo-Leaf Hierarchical Structure. *Journal of Materials Chemistry A* **8**, 17449–17453 (2020).
- DuChene, J. S. et al. Prolonged Hot Electron Dynamics in Plasmonic-Metal/Semiconductor Heterostructures with Implications for Solar Photocatalysis. *Angewandte Chemie International Edition* **53**, 7887–7891 (2014).
- Clatworthy, E. B. et al. Enhanced Photocatalytic Hydrogen Evolution with TiO<sub>2</sub>-Tin Nanoparticle Composites. *The Journal of Physical Chemistry C* **123**, 3740–3749 (2019).
- Nguyen, N. T. et al. Enhanced Co<sub>2</sub> Photocatalysis by Indium Oxide Hydroxide Supported on Tin@TiO<sub>2</sub> Nanotubes. *Nano Letters* **21**, 1311–1319 (2021).
- Li, C., Yang, W., Liu, L., Sun, W. & Li, Q. In Situ Growth of TiO<sub>2</sub> on Tin Nanoparticles for Non-Noble-Metal Plasmonic Photocatalysis. *RSC Advances* **6**, 72659–72669 (2016).
- Kim, S. et al. Wifi-Like Nanostructures from Confinement of Block Copolymer Microdomains in Asymmetric Hemisphere Nanocavity. *Macromolecules* **56**, 1837–1844 (2023).
- Kim, S. et al. Self-Assembled Pagoda-Like Nanostructure-Induced Vertically Stacked Split-Ring Resonators for Polarization-Sensitive Dichroic Responses. *Nano Convergence* **9**, 40 (2022).
- Lee, D. et al. Sub-Ambient Daytime Radiative Cooling by Silica-Coated Porous Anodic Aluminum Oxide. *Nano Energy* **79**, 105426 (2021).
- Cao, Z. L. & Ong, H. C. Determination of the absorption and radiative decay rates of dark and bright plasmonic modes. *Opt. Express* **22**, 16112 (2014).
- Baah, M. et al. All-graphene perfect broadband THz absorber. *Carbon* **185**, 709 (2021).
- Gómez, D. E. et al. The Dark Side of Plasmonics. *Nano Lett* **13**, 3722 (2013).
- Gallinet, B. & Martin, O. J. F. Ab initio theory of Fano resonances in plasmonic nanostructures and metamaterials. *Phys. Rev. B* **83**, 235427 (2011).
- Hoeing, D., Schulz, F., Mueller, N. S., Reich, S. & Lange, H. Dark plasmon modes for efficient hot electron generation in multilayers of gold nanoparticles. *J. Chem. Phys.* **152**, 064710 (2020).
- Yong, Z., Zhang, S., Gong, C. & He, S. Narrow Band Perfect Absorber for Maximum Localized Magnetic and Electric Field Enhancement and Sensing Applications. *Scientific Reports* **6**, 24063 (2016).
- Lee, D. et al. Multiple-Patterning Colloidal Lithography-Implemented Scalable Manufacturing of Heat-Tolerant Titanium Nitride Broadband Absorbers in the Visible to near-Infrared. *Microsystems & Nanoengineering* **7**, 14 (2021).
- Smith, D. R., Vier, D. C., Koschny, T. & Soukoulis, C. M. Electromagnetic Parameter Retrieval from Inhomogeneous Metamaterials. *Physical Review E* **71**, 036617 (2005).
- Liu, T., Wang, Q., Zhang, C., Li, X. & Hu, J. High Performance of Hot-Carrier Generation, Transport and Injection in Tin/TiO<sub>2</sub> Junction. *Frontiers of Physics* **17**, 53509 (2022).
- Doiron, B. et al. Plasmon-Enhanced Electron Harvesting in Robust Titanium Nitride Nanostructures. *The Journal of Physical Chemistry C* **123**, 18521–18527 (2019).
- Patsalas, P. & Logothetidis, S. Optical, Electronic, and Transport Properties of Nanocrystalline Titanium Nitride Thin Films. *Journal of Applied Physics* **90**, 4725–4734 (2001).